

Tabletop imaging of structural evolutions in chemical reactions

Heide Ibrahim¹, Benji Wales², Samuel Beaulieu¹, Bruno E. Schmidt¹, Nicolas Thiré¹, Éric Bisson¹, Christoph T. Hebeisen^{3,4}, Vincent Wanie¹, Mathieu Giguère¹, Jean-Claude Kieffer¹, Joseph Sanderson², Michael S. Schuurman³, François Légaré¹

1. *Institut National de la Recherche Scientifique, Centre Énergie Matériaux et Télécommunications, 1650 Boulevard Lionel-Boulet, Varennes, Qc, J3X1S2, Canada*

2. *Department of Physics and Astronomy, University of Waterloo, 200 University Avenue West, Waterloo, ON N2L 3G1, Canada*

3. *National Research Council of Canada, 100 Sussex Dr., Ottawa, K1A 0R6, Canada*

4. *Department of Physics, University of Ottawa, 150 Louis Pasteur, Ottawa ON, K1N 6N5, Canada*

The introduction of femto-chemistry has made it a primary goal to follow the nuclear and electronic evolution of a molecule in time and space as it undergoes a chemical reaction. Using Coulomb Explosion Imaging we have shot the first high-resolution molecular movie of a to and fro isomerization process in the acetylene cation. So far, this kind of phenomenon could only be observed using VUV light from a Free Electron Laser [*Phys. Rev. Lett.* 105, 263002 (2010)]. Here we show that 266 nm ultrashort laser pulses are capable of initiating rich dynamics through multiphoton ionization. With our generally applicable tabletop approach that can be used for other small organic molecules, we have investigated two basic chemical reactions simultaneously: proton migration and C=C bond-breaking, triggered by multiphoton ionization. The experimental results are in excellent agreement with the timescales and relaxation pathways predicted by new and definitively quantitative ab initio trajectory simulations.

26 Since the introduction of femto-chemistry¹⁻⁵, electron or X-ray diffraction have been the
27 most commonly employed techniques to track nuclear rearrangement in molecules⁶⁻⁹.
28 Unfortunately, these techniques are largely insensitive to the more subtle and irregular structural
29 changes that can occur within a single small molecule undergoing a chemical reaction. Pump-
30 probe Coulomb Explosion Imaging (CEI) allows observation of these changes on a femtosecond
31 (fs) timescale with atomic resolution¹⁰⁻¹³. So far, however, important phenomena such as proton
32 migration in the acetylene cation, have only been observed using VUV light from a Free
33 Electron Laser (FEL)¹⁴. It will be presented here that results obtained in a tabletop multiphoton
34 approach can go well beyond those FEL results, including a high resolution molecular movie of
35 proton migration from the linear acetylene cation ($[\text{HC}=\text{CH}]^+$) to the vinylidene cation ($[\text{C}=\text{CH}_2]^+$).

36 Since laser driven tunnel ionization preferentially ionizes a neutral molecule to the
37 electronic ground state of the cation, any subsequent nuclear dynamics will generally occur on
38 that state. The ability to readily initiate dynamics on an excited electronic state of the cation
39 would enable a variety of new and complex experiments. Employing the intuitive Koopman's
40 approximation picture of ionization¹⁵, the ground electronic state of a cation is generated by
41 removal of an electron from the highest molecular orbital (HOMO) of the neutral, while excited
42 states are generated by ionizing electrons from the lower-lying HOMO-n orbitals. It had for
43 example been assumed that only ionization of the HOMO contributes to High Harmonic
44 Generation (HHG) – because of the low frequency fields used. However, recent results,
45 obtained at 800 nm, demonstrate that ionization of HOMO-n orbitals may also contribute to an
46 HHG spectrum¹⁶⁻¹⁸. Given the coherent nature of HHG process, even a small excited state
47 contribution can have a significant impact on the observed signal due to interference effects.
48 However, in CEI these contributions add linearly, and thus a small contribution from ionization of
49 the HOMO-n would be difficult to observe.

50 To efficiently launch dynamics in excited states of molecules with a large energy gap
51 between ground and excited states it is common to use high photon energy sources such as
52 FELs (acetylene)¹⁴ or HHG (ethylene)¹⁹. If sub-fs resolution is required, one can use an XUV
53 pump/XUV probe arrangement based on HHG for this kind of experiments^{20,21}, however at the
54 price of a highly demanding experimental setup. Here we show that multiphoton ionization with
55 ultrashort UV laser pulses provides a powerful alternative to demanding VUV sources.

56 Even though acetylene (C₂H₂) has been serving as a model system for decades, proton
57 migration dynamics in its cation is not yet fully elucidated and has recently attracted attention of
58 both experimental and theory groups^{12-14,22-24}. Given its small size, it is an ideal candidate for
59 the application of quantitative electronic structure theory, which can be brought to bear on its
60 ground and excited states.

61 Actually, proton migration pumped by 800 nm pulses has been observed solely in the
62 dication of deuterated acetylene by Hishikawa and coworkers^{12,13}. Very recently, optimal control
63 experiments confirmed that excitation with 800 nm pulses leads to isomerization in the dication²⁵.
64 These 800 nm pump schemes, however, are not capable of launching proton migration in other
65 charge states such as in the cation²⁶.

66 This is because it is quite challenging to overcome the potential energy barrier of 2 eV²⁷
67 which separates the acetylene cation in its ground state X²Π_u from vinylidene, as indicated in
68 the experimental scheme of Figure 1. Therefore, to obtain sufficient energy to overcome this
69 isomerization barrier²², it is necessary to populate the A-state (A²Σ_g⁺) of [HC=CH]⁺ (5.8 eV
70 above the ground state), which requires ionization from the HOMO-1. This cannot be achieved
71 in the adiabatic regime with 800 nm pulses²⁶. To remain in the adiabatic regime for long
72 conjugated molecules that display small energy gaps, Lezius et al.²⁸ have suggested increasing
73 the laser wavelength. Inverting this idea, it appears sensible to reach the non-adiabatic regime

74 for small molecules by employing UV wavelengths with larger photon energies. Here we present
75 a generalized approach using 266 nm pump pulses that unites the convenience and flexibility of
76 a tabletop setup with excitation ranges of FELs – and unveils the isomerization process in
77 unprecedented detail allowing us to record a molecular movie. This movie shows for the first
78 time, that multiple oscillations can occur between the two isomers acetylene and vinylidene.

79 This paper is structured as follows: Firstly, in a single pulse experiment we verify that
80 excitation with 266 nm pulses leads to the same spectral signatures as those obtained with an
81 FEL¹⁴, confirming that we populate the first excited electronic state of the acetylene cation
82 ($A^2\Sigma_g^+$) which initiates proton migration. Secondly, we present time-resolved pump probe
83 experiments of the two-body breakup. Based on the single-pulse experiments, the presence of
84 CH_2^+ in the dynamics of the vinylidene channel in the cation ($C^+CH_2^+$ correlation) is a clear
85 indicator of proton migration since one proton has been migrating to the other side of the
86 molecule. In addition to proton migration resulting in the formation of bound vinylidene
87 molecules in the cation, new channels that lead to dissociation of the cation are observed in
88 both, the vinylidene and the acetylene (CH^+CH^+) correlations. And thirdly, we investigate the
89 three-fragment correlations from the same experimental data set ($C^+CH^+H^+$) and construct a
90 molecular movie of proton migration, which exhibits excellent agreement with new numerical
91 simulations of nonadiabatic wavepacket propagation on the ground and excited electronic states
92 of the cation. These *ab initio* trajectory simulations employ definitive levels of electronic
93 structure theory in the description of the relevant potential energy surfaces.

94 **SINGLE PULSE EXPERIMENT.** Signatures of proton migration in $C_2H_2^+$ have recently
95 been demonstrated at the FEL in Hamburg¹⁴ with XUV light (38 eV). Indications of time
96 dependent acetylene – vinylidene isomerization, photoinitiated via ionization to the A-state of
97 the acetylene cation appear in the kinetic energy release (KER) of correlated C^+ and CH_2^+
98 fragments at energies above 5.8 eV¹⁴. As an initial experiment we set out to find this signature

99 by employing single laser pulses of 266 nm central wavelength and varying pulse duration and
100 peak power. The experimental scheme in terms of relevant electronic and ionic states and
101 excitation pathways is described in Figure 1. The A-state of the acetylene cation is reached by
102 absorption of four 266 nm photons (corresponding to $4 \times 4.66 \text{ eV} = 18.64 \text{ eV}$). Once on the A-state,
103 proton migration occurs, which is then followed by ionization to a dissociative state of the
104 dication within the same laser pulse. Results of a single 266 nm pulse experiment are shown in
105 Figure 2a), containing the KER distributions of the two-fragment correlation channel of
106 vinylidene for 32 fs (green and red), 110 fs (black) and 250 fs (blue) pulse duration and various
107 pulse powers. Already a short pulse of moderate pulse power (green solid line) leads to a KER
108 distribution broadened on the high energy side. With increasing pulse duration a strongly
109 pronounced high-energy shoulder appears. The shoulder obtained with 250 fs pulses (blue solid
110 line) agrees very well with data obtained at the FEL using 38 eV (open circles)¹⁴. This shoulder
111 was assigned to proton migration initiated by ionizing acetylene to the A-state of its
112 cation^{14,22,24,29}. The proton migration which we observe is essentially pulse duration dependent
113 and only secondarily intensity dependent. The pulse powers of the short 32 fs pulse ($1 \cdot 10^8 \text{ W}$
114 and $2 \cdot 10^8 \text{ W}$), which are higher by a factor of five than those for the long pulse, indicate that
115 increasing the intensity alone will not lead to a strongly pronounced high energy shoulder.
116 Fragmentation occurs in the doubly charged state which is accessed here in a sequential
117 process within a single pulse. This effect is therefore most pronounced for the longest pulses
118 (250 fs) which are also of the lowest power.

119 Additionally, we employed 800 nm, 200 fs pulses (grey shaded). The energetically
120 narrow KER distribution from 800 nm excitation confirms the observation of Alnaser et al.²⁶. In
121 this case, we do not obtain high energy fragments as a signature of isomerization in the
122 acetylene cation and similar results were obtained at 400 nm (not shown). This was a primary

123 motivation for our study at 266 nm in order to confirm that UV excitation is essential to populate
124 the A-state.

125 **INITIAL STATE ASSIGNMENT – I.** Assignment of the electronic states involved in the
126 isomerization can be more demanding in a multiphoton scheme compared to a single photon
127 scheme pumped by one VUV photon. In both cases however, multiple states can be populated,
128 e.g. the ground and the first excited state of the cation. In our experiment, while the cationic A-
129 state is excited by four photons, the ground state of the cation $X^2\Pi_u$ is populated in a three
130 photon process. However, the documented energy barrier separating the acetylene and
131 vinylidene isomers will prohibit proton migration from low-lying vibrational levels on the
132 electronic ground state²⁷, so its contribution will only show up around the main peak of KER in
133 Figure 2a). To confirm that the experimentally observed high energy shoulder arises from
134 ionization to the A-state¹⁴, we investigate the angular distribution of the molecular fragments
135 from the KER spectrum obtained with the 110 fs, 266 nm pulse shown as a black solid line in
136 Figure 2a). Initially, all population is in the $X^1\Sigma_g^+$ electronic state of the neutral acetylene.
137 Following Koopman's approximation¹⁵, ionization to the $A^2\Sigma_g^+$ state of the acetylene cation
138 requires the removal of one electron from the HOMO-1, which is a σ_g orbital. The probability for
139 ionization from this orbital is largest for those molecules aligned parallel to the polarisation of the
140 laser field¹⁷ (this corresponds to the angle $\theta=0^\circ$, consistent with the definition given in the inset
141 of Figure 1). Note that this is exactly where the maximum in the high energy shoulder of the
142 angular resolved KER distribution is observed (see cyan shaded curve of Figure 2b). The high
143 energy maximum of this particular angular slice is significantly more pronounced than for all
144 other angular distributions and even exceeds the main peak. Thus, we can confidently assign
145 this region to ionization to the $A^2\Sigma_g^+$ state. Although higher electronic states with Σ symmetry
146 exist in the cation, the probability of them being populated under the current experimental

147 condition is significantly lower than for the A-state (see section II. in the supplementary
148 information – SI).

149 **PUMP PROBE EXPERIMENT – TWO BODY BREAKUP.** Next, we employed pump-probe
150 CEI to image the dynamics resulting from multiphoton ionization with 266 nm pulses. We
151 investigate two chemical reactions: i) proton migration – one of the fundamental processes in
152 chemistry and biology, and ii) the first observation of C=C bond breaking on highly excited
153 states of the acetylene and vinylidene cation.

154 We focus first on the isomerization process: As shown in the experimental scheme of
155 Figure 1, a 266 nm pump-pulse ionizes the system to $[\text{HC}=\text{CH}]^+$ in a four-photon process
156 thereby initiating proton migration dynamics. A time delayed, 800 nm probe-pulse tunnel-ionizes
157 the molecule to doubly and triply charged states of acetylene or vinylidene. Its electric field
158 stripes off electrons, leaving behind positively charged fragments which undergo Coulomb
159 explosion. As in the single pulse experiments, proton migration dynamics shows up in pump-
160 probe experiments in the high-energy region obtained by correlating two fragments. This
161 dynamics corresponds to the region V3 of the vinylidene channel ($\text{C}^+\text{+CH}_2^+$) in Figure 3a). We
162 observe an increase of the yield in this high energy shoulder in the temporal window of 60-100
163 fs followed by a decrease. (We will leave the details about the proton migration dynamics and
164 vinylidene formation until we have direct evidence from three fragment correlations of Figure 5
165 and Figure 6.) Note that this high energy shoulder is less pronounced in the pump-probe
166 experiment of Figure 3 compared to the single pulse experiment in Figure 2a), in which the
167 complete two-step ionization process occurs many times beneath a single pulse envelope.
168 Therefore, for long single pulse durations (110 and 250 fs) the excited state dynamics can be
169 initiated on a larger number of molecules and this gives rise to an accumulated vinylidene
170 formation, compared to the 32 fs in case of the pump-probe experiment.

171 The mid-energy region V2 in Figure 3a) has been previously¹⁴ assigned to a
172 sequential double ionization. In addition we observe a new peak emerging in the low-energy
173 region V1. This peak is first visible around 80 fs, and has, to our knowledge, never been
174 observed before for $C_2H_2^+$. Since it occurs for both vinylidene and acetylene ($CH^+ + CH^+$, Figure
175 3b), we attribute it to a stretching of the C=C bond. In both channels it migrates to smaller
176 energies (indicating an increase in the C-C internuclear distance) with increasing time delay.
177 The peak strength continuously increases with increasing time delay, which is consistent with a
178 lowering of the ionization potential as the C=C bond length increases.

179 Employing Coulomb potentials for analysis, the peak at 1 eV corresponds to an
180 elongation of the C=C bond to $> 4 r_{eq}$, where r_{eq} is the equilibrium distance, implying that the
181 molecule has largely dissociated. Similar dissociation effects have been observed in $C_2H_2^{2+}$ ³⁰
182 and 1,3-butadiene³¹. While none of the low lying electronic states of $C_2H_2^+$ is dissociative along
183 the C-C stretch coordinate, if a fifth photon is absorbed during the pump-pulse, the molecule will
184 have energy in excess of the lowest C-C dissociation asymptotes (see Figure 1 and Figure S9
185 in the SI). Since the dissociation dynamics occur in both the acetylene and vinylidene channels
186 they are likely to be triggered by the same event, namely absorption of a photon to higher lying
187 excited states of the cation. From there it can proceed to dissociative states of the vinylidene
188 cation. This dissociation pathway has not been observed at a FEL¹⁴ given that for one-photon
189 absorption, once ionized, no further coupling between electronic states occurs. We predict that
190 in a multiphoton experiment with shorter pump-pulses this sequential coupling after ionization is
191 also likely to be suppressed.

192 **THREE BODY BREAKUP.** This new dissociation channel also shows up in the three-body
193 breakup $C_2H_2^{3+} \rightarrow H^+ + C^+ + CH^+$, in which two electrons are removed by the probe pulse. Before
194 we address the rich information present in this channel though, we first need to prove that it is
195 indeed what we claim and that the probe pulse is only showing us dynamics of the cation. As a

196 first step in doing so, we compare the KER features in the two-body channel (Figure 3), which
197 we have established to show us time dependent processes which must originate in the cation,
198 with those of the three-body channel in Figure 4. Panel a) contains the total kinetic energy
199 released during the Coulomb explosion. The peak maximum migrates from approximately 15 eV
200 at time zero to 7 eV at a time delay of a picosecond, indicating the presence of the dissociative
201 channel described in the previous section. To uncover the close analogy between two- and
202 three-body breakup we take advantage of the fact that in the three-body channel an H^+ fragment
203 is created, which, because of conservation of momentum, is responsible for carrying away most
204 of the increased and broadband energy release. If the 3+ channel is observing the same
205 dynamics, we expect strong similarities in the energy sum of correlated $C^+ + CH^+$ fragments of
206 the three-body channel, with the total energy released in the two-body channel. To extract
207 hidden sub-structures of Figure 4a) we look at the 3+ KER reduced by the proton energy in b),
208 leading to a double peak structure with one peak around 6 eV and another one emerging for
209 longer times and moving to 1 eV at one picosecond. The overall KER is still slightly higher
210 compared to the two-body breakup since here Coulomb potentials are more closely
211 approximated. The key difference being that while both of the main peaks are well separated in
212 the two-body case, the peaks in Figure 4b) are much broader, leading to an overlap of the
213 dominant spectral features. This is due to the additional broadband energy both, the CH^+ , and
214 the C^+ fragments gather when the proton is removed from either CH_2^+ or CH^+ . The temporal
215 evolution of the kinetic energy released by the single fragments is shown in Figure S3 of the SI,
216 which indicates, that apart from the C-C bond also the C-H bond dissociates. The low energy
217 peak in Figure 4 follows precisely the evolution that was observed for the peak assigned to
218 dissociation in the two-body breakup in Figure 3. This constitutes strong evidence that we
219 observe the same cation dynamics in the two-body and in the three-body-breakup. The KER
220 spectra for the three-body breakup are too broad to clearly observe the high energy shoulder
221 associated with the launching of proton migration. However, since dissociation in the cationic

222 states requires the absorption of a fifth photon, compared to the four photons required to initiate
223 proton migration dynamics on the A-state, it is most likely that the latter process as well is
224 initiated on the cation and probed via ionization to the triply charged states.

225 In the three-body breakup channel we have access to the direction in which the
226 proton is emitted, allowing us to follow the proton migration process in detail. At its simplest, if
227 the proton trajectory is close to the direction of the CH^+ fragment, it means that the molecule
228 was close to the vinylidene isomer when Coulomb exploding. While, if the proton is close to the
229 C^+ fragment direction, the molecule is closer to acetylene. Such an analysis allows for the
230 construction of a molecular movie of the proton migration reaction, where key frames are
231 represented by the Newton plots in Figure 5 as described in the figure caption. Since proton
232 migration in the acetylene cation initiated on the A-state results in a bound vinylidene cation (*i.e.*
233 non-dissociative), its Coulomb explosion will yield in a high KER. Therefore, the dynamics of
234 interest were isolated by filtering the total three-body KER data, selecting only those correlated
235 events above 13 eV, thereby excluding the C-C bond dissociation events visible in Figure 3 and
236 Figure 4. The cut-off for energy filtering is indicated as a black line in Figure 4a). For
237 comparison, unfiltered Newton plots are presented in Figure S5 in the SI. In Figure 5 proton
238 fragment momenta are presented in the molecular frame³², in concert with classically calculated
239 values (shown as symbols) which assume Coulomb potentials and are included to serve as a
240 visual guide. Despite substantial deviations of triply charged states from a Coulomb potential,
241 the agreement between this simple calculation and the experimental data is very good. Starting
242 from the linear geometry of neutral acetylene in the ground-state, the trans-configuration is
243 reached after 20 fs, indicated by a depletion in signal at $(x=-1.0|y=0.0)$ which is shown in blue
244 and an increased signal at $(x=-0.3|y=0.7)$ shown in green. This matches a half-period of the
245 trans-bent vibrational mode. At 40 fs the centre of mass reaches the classically calculated
246 transition state $(x=0.0|y=1.0)$. This agrees with timescales predicted by our semi-classical

247 simulations for a population transfer to the ground state mediated by the conical intersection. A
248 maximum in vinylidene formation (classically calculated value ($x=0.6|y=0.8$)) is observed around
249 100 fs, after which the population maximum swings back to the acetylene side (with a vinylidene
250 population minimum around 150 fs). This oscillation continues, with the next vinylidene
251 population maximum observed at 180 fs. All time values are associated with an error of ± 5 fs.

252 The to and fro isomerization behaviour of Figure 5 is perfectly reproduced by the *ab*
253 *initio* trajectory simulations of the vibronic dynamics, as evinced in Figure 6. While a single
254 recurrence had also been observed in $C_2D_2^{2+}$ ^{12,13} we now see further oscillations associated
255 with the evolution of the nuclear wavepacket. We deduce from these results the following proton
256 migration process: Both, X- and A-states are populated in a three-, and four-photon process,
257 respectively (Figure 1). According to our calculations and Ref. [22], the A-state population is
258 depleted by roughly half in the first 40-50 fs via a trans-bent conical intersection to hot
259 vibrational states of the ground electronic state of $[HC=CH]^+$. Formation of vinylidene takes
260 place exclusively here, where the isomerization barrier can be overcome in both directions,
261 which is why we observe the to and fro isomerization between acetylene and vinylidene (see
262 green arrow in Figure 1). The initial X-state population does not contribute to isomerization since
263 its energy is too low to overcome the isomerization barrier. The isomerization process itself is
264 'primed' by the pre-eminence of motion along the trans-bending mode in the excited state (see
265 Figures S6-S8 in the SI). The solid lines in Figure 6 represent the total ground- and excited-state
266 populations of acetylene (red) and vinylidene (blue) cation, as elucidated in the SI. As evinced in
267 Figure 6, the agreement is excellent up to 150 fs. From a single exponential fit we estimate the
268 initial isomerization time to be approximately 41 fs (theory) and 43 ± 10 fs (experiment), in accord
269 with previous results¹⁴. The temporal resolution achieved, results from the fact that both, the
270 pump and the probe step are highly nonlinear (see Figure S2 in the SI).

271 **INITIAL STATE ASSIGNMENT – II.** In order to validate the proposed interpretation of the
272 three-fragment correlation data, we confirm that the imaged dynamics occur on the state of
273 interest – *i.e.* the A-state of the cation. Evidence for a low-lying electronic state of Σ symmetry
274 (such as the A-state) has already been presented in the single pulse experiments of Figure 1
275 with the appearance of a high energy shoulder analogous to observations at the FEL and its
276 angular dependence, which reveals ionization from the HOMO-1. While Coulomb explosion
277 occurs in the triply charged molecule $C_2H_2^{3+}$, there exist multiple combinations of pump and
278 probe pulses that may be employed to reach this ionic state. To verify that it is indeed dynamics
279 on the cationic state that are being probed rather than the neutral or the subsequently prepared
280 dicationic surface, we first note that we expect negligible dicationic populations to be prepared
281 by the pump step since the ratio of parent ion $C_2H_2^+$ to $C_2H_2^{2+}$ in the TOF spectrum is $> 100:1$,
282 demonstrating that the pump step strongly favours preparation of the cation over the dication.
283 Additionally, neither pump- nor probe-pulses alone contribute more than 0.3% to the correlated
284 counts of the two-body breakup, compared to their joined interaction. Of course, our method is
285 only sensitive to the combination of pump and probe step, and thus an extremely efficient (but
286 here undesirable) probe step for the transition from the $2^+ \rightarrow 3^+$ states, compared to the $1^+ \rightarrow 2^+$
287 could in principle compensate for the pump efficiency. We therefore estimated the tunnel
288 ionization rates for these processes based on the Keldysh-theory (see section III. in the SI). The
289 results show the $1^+ \rightarrow 2^+$ ionization process to be >100 times more efficient than the $2^+ \rightarrow 3^+$
290 ionization. Thus the limiting factor in the probe step is the ionization from $2^+ \rightarrow 3^+$ – a barrier
291 which is overcome, since we are observing the breakup of a triply charged molecule. These
292 calculations also suggest that $1^+ \rightarrow 2^+$ process is near saturation employing the laser intensities
293 used here. The latter point is consistent with (and perhaps a necessary precondition for) the
294 observation of the triply charged species. Combining the efficiencies of pump and probe step it

295 appears therefore extremely unlikely that we observe dication dynamics in the case of three-
296 fragment correlation – which is also supported by the fact that the same dissociation dynamics
297 is observed both in the dication (Figure 3) and the trication (Figure 4), as discussed earlier.
298 Further, dynamics in neutral C_2H_2 can also be excluded on the basis of the power dependence
299 measurement of the single 266 nm pulse experiment presented in Figure S1 of the SI. While for
300 low pump powers we observe a four-photon absorption which matches the ionization potential
301 of the A-state energetically, for higher pump powers it is indicated that we are driving the pump
302 step in saturation. This saturation effect also holds for the experimental condition of the pump-
303 probe experiment. Thus, by the arrival time of the probe-pulse, there are no neutral molecules
304 left in the jet. Additionally, the identity of the KER of a CH^+ fragment from the two-body breakup
305 with an uncorrelated CH^+ fragment, as discussed in Figure S4 of the SI, further indicates, that
306 we are probing dynamics in the cation. Finally, this assignment is strongly supported by the
307 excellent agreement with new high-level theoretical simulations of the $C_2H_2^+$ A-state initiated
308 dynamics, as shown in Figure 6.

309 In summary, if one aims to populate the excited states of charged molecules whose
310 difference in ionization potentials is too large to be overcome by 800 nm photons, our
311 experimentally rather simple approach provides an alternative to demanding VUV sources.
312 Indeed, given the limited availability, repetition rate, pulse stability and timing jitter of FELs, our
313 approach provides tremendous benefits in terms of statistics and temporal resolution.
314 Combining pump-probe CEI with multiphoton absorption of UV light opens the door to time-
315 resolved imaging of chemical reactions and very rich dynamics since a variety of electronic
316 states is accessed simultaneously. Careful consideration, as here, makes it possible to identify
317 their origins unambiguously. Combined with theoretical simulations, our results present the most
318 complete picture of proton migration and C=C bond breaking on the ground and excited states
319 of $C_2H_2^+$ to date.

320 **METHODS**

321 **Experimental technique:** Experiments were carried out at the Advanced Laser Light Source
322 ALLS (INRS-EMT, Varennes, Canada). We employ pump-probe CEI: A pump-pulse (266 nm,
323 32 fs, 3.2 μJ) ionizes the system to the cation and launches proton migration dynamics. A time
324 delayed probe-pulse (800 nm, 40 fs, 44 μJ) further ionizes it to higher charged states. Its electric
325 field stripes-off electrons almost immediately, leaving positively charged fragments behind which
326 undergo Coulomb explosion. They represent the molecule's geometric configuration at the
327 arrival time of the probe-pulse. The strength of CEI is its ability to directly image geometrical
328 structures. It does not provide direct observation of electronic states, as photoelectron
329 spectroscopy would do. Nevertheless, we are able to draw conclusions about the electronic
330 states populated in the initial ionization from the angular distribution of the molecular fragments
331 and theoretical support.

332 Intense 266 nm pulses were obtained by sum frequency generation of the fundamental
333 beam (800 nm, 2.5 KHz, 35 fs, KM labs) with its second harmonic (400 nm) in a 40 μm thick
334 type I BBO crystal (Altos Photonics). Pulse duration was controlled by chirped mirrors (Ultrafast
335 Innovation) and/or fused silica plates from almost Fourier-transform limited (32 fs) to above 250
336 fs. Measurements were obtained with a homebuilt TG-FROG³³. Pulse energy was varied
337 between 11.2 μJ and 3.2 μJ . For the pump-probe experiments a 32 fs, 3.2 μJ pump-pulse of
338 266 nm was combined with a 40 fs, 44 μJ probe-pulse of 800 nm. Laser polarization was
339 vertical for both, pump- and probe-beams. Laser pulses were focussed ($f=100$ mm) into a
340 collimated acetylene gas jet (Praxair AC 2.6AA-A5). Pump intensity on target was estimated to
341 3×10^{14} W/cm². Ionic fragments resulting from Coulomb explosion are collected with a uniform-
342 electric-field ion imaging spectrometer. Their full 3D momenta are retrieved using a time-and-
343 position-sensitive delay line detector at the end of the 23 cm ion time of flight (TOF)
344 spectrometer (RoentDek Handels GmbH). Due to the vertical polarisation direction two

345 fragments of same mass and charge but opposite momenta (e.g. CH^+/CH^+ , the acetylene
346 channel) will hit the same detector position – but at different times. Thus choosing the correct
347 TOF range enables us to distinguish them.

348 Due to a significantly increased intensity when pump- and probe-pulses overlap temporally, the
349 effective focal volume is increased within which the threshold for ionization is reached, leading
350 to an increase in ionized molecules. This allows determining time zero by the appearance of a
351 60% increase in total ion yield (sum of all ion fragments) when scanning the delay stage. Error
352 of time zero assignment is around ± 5 fs, partially due to drifts over typical acquisition times of
353 24-48 h. Even though the pulse durations of 32 fs and 40 fs for pump- and probe-pulses appear
354 quite long, we like to point out that both – pump and probe step – are highly non-linear. A four-
355 photon excitation effectively shortens the pump-pulse to 16 fs and also the effective tunnel
356 ionization time for the probe-pulse will be much shorter than the actual pulse duration.

357 **Data analysis:** Due to the large count rates produced in this experiment (typically > 3 ions per
358 laser shot), a sophisticated algorithm is used to parse the data for true coincidences³⁴. A TOF
359 window is defined in order to identify events registered by the position sensitive detector as
360 specific ions – either H^+ , C^+ , CH^+ , CH_2^+ , or CC^+ . The data is then parsed, laser shot by laser
361 shot, for the existence of a specific fragmentation channel - e.g. (H^+ , C^+ , CH^+) for the three-body
362 breakup, or for the two-body breakup (CH^+ , CH^+) as the acetylene channel and (C^+ , CH_2^+) giving
363 the vinylidene channel. If data from a laser shot yields the desired ions for the fragmentation
364 channel, the momentum for these ions is calculated. If the momentum sum is near zero ($< 10^{-23}$
365 kg m/s), the group of ions is considered a true coincidence, originating from the same molecule.
366 The momentum information for this channel is stored for further calculation of various metrics –
367 e.g. KER, θ (see inset Figure 1), etc. It is possible with these high count rates that multiple ions
368 are detected in the TOF windows defined for a specific channel, leading to several possible

369 combinations of ions – the majority of which are false. In this case, all ion combinations are
370 considered and only that which yields near zero momentum is stored as a true coincidence.

371 **Theoretical methods:** The excited nonadiabatic molecular dynamics on the $A^2\Sigma_g^+$ state were
372 simulated using the full multiple spawning approach³⁵ – a semiclassical method. In this
373 methodology, the vibronic wavepacket is represented in a basis of direct products (over each
374 Cartesian coordinate) of frozen Gaussian functions. These basis functions, or trajectories, are
375 propagated classically, with the potential energy surfaces determined “on-the-fly” using *ab initio*
376 electronic structure methods. The number of trajectories expands dynamically, to account for
377 regions of nonadiabatic coupling between electronic states, by “spawning” (approximating non-
378 adiabatic transitions) new basis functions onto different electronic states as needed. The
379 requisite energy gradients and derivative couplings required to propagate the trajectories were
380 computed at a very high level of electronic structure theory, employing atomic natural orbital
381 (ANO) basis sets and a first-order multireference configuration interaction (FO-MRCI) treatment
382 of electron correlation³⁶. The underlying complete active space (CAS) reference functions for
383 the MRCI procedure were determined employing a 7 electron, 7 orbital (7e,7o) active space.
384 The initial distribution of nuclear positions and momenta for the simulation were generated by
385 sampling the ground vibrational state of neutral acetylene³⁷. From 20 initial conditions, 1480
386 spawned trajectory basis functions were generated. On the basis of these simulations, the
387 adiabatic state populations as a function of time, as well as the geometric character of the
388 wavepacket (*i.e.* acetylenic vs. vinylidenic) could be readily determined. Details on the
389 theoretical methods are provided in the supplementary information.

390 Assuming a Coulomb potential for the 3⁺ charge state ($C_2H_2^{3+} \rightarrow C^+ + CH^+ + H^+$),
391 momentum positions within the Newton plot have been calculated for four structures using
392 classical mechanics; (1) C_2H_2 at equilibrium, (2) $C_2H_2^+$ in the trans geometry, (3) $C_2H_2^+$ at the
393 transition state at the conical intersection, and (4) $C_2H_2^+$ in vinylidene geometry. For the CH^+

394 fragment, it is assumed that the charge is located on the carbon with a mass of 13. The initial
395 velocities of the fragments are assumed to be zero. Geometrical structures were obtained using
396 the level of theory described above.

397

398 **Acknowledgement**

399 The authors gratefully acknowledge supportive discussions with Dr. Michael Spanner and
400 research funding from NSERC, FQRNT and CIPI. H.I. acknowledges financial support from the
401 NSERC-Banting Postdoctoral Fellowships Program. S.B. and V.W. are thankful for financial
402 support from NSERC.

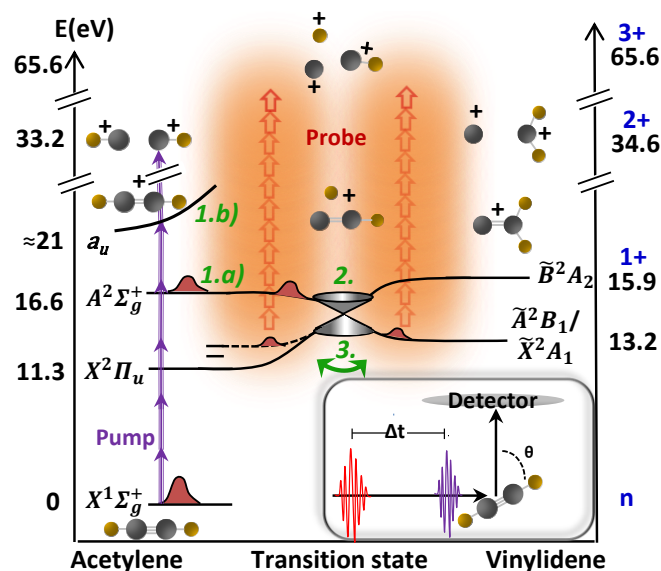
403 **Author contribution:**

404 H.I. and F.L. designed the experiment, H.I., B.W., S.B., B.E.S., N.T., E.B., M.G., C.H., and J-
405 C.K. carried out the experiments, M.S.S. and F.L. provided the theoretical support, H.I., B.W.,
406 S.B., V.W., M.S.S., J.S., and F.L. carried out data analysis and interpretation, H.I., F.L., M.S.
407 and J.S. wrote the manuscript, with support from all other authors.

408 **Additional information**

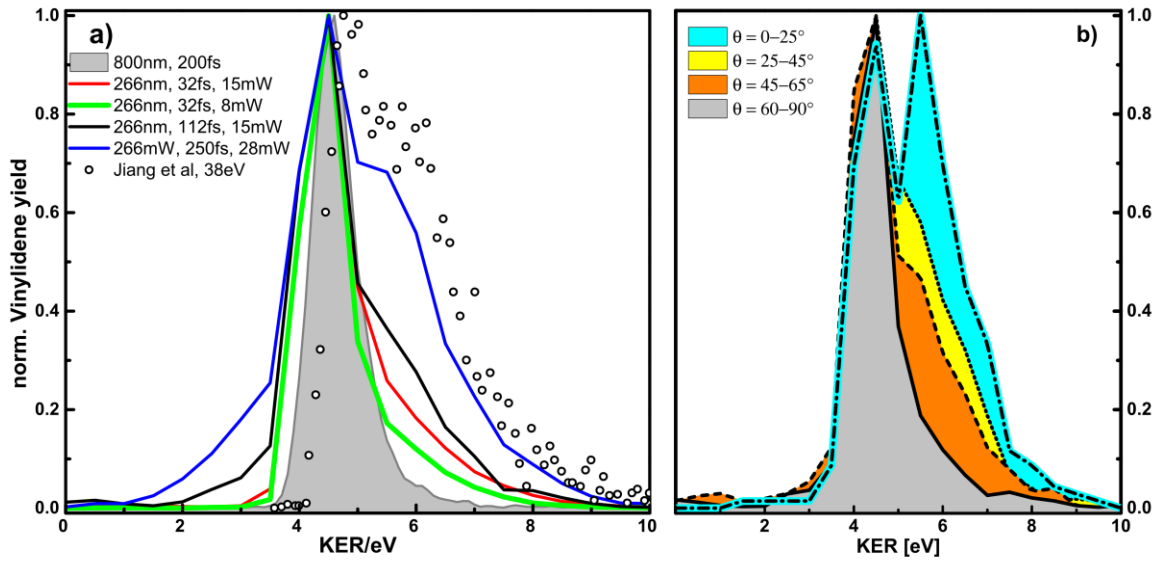
409 The authors declare no competing financial interests. Supplementary information
410 accompanies this paper. Correspondence and requests for materials should be addressed to
411 H. I. and F. L.

412



413

414 **Figure 1 – Experimental scheme:** (1.a) A 266 nm pump-pulse populates the first excited state $A^2\Sigma_g^+$ of $[\text{HC}=\text{CH}]^+$ in
 415 a four-photon ionization process. *Proton migration pathway:* (2.) Within 40 fs the wavepacket enters a region of
 416 strong nonadiabatic coupling with the ground $X^2\Pi_u$ state of $[\text{HC}=\text{CH}]^+$ (1+). Passage through this region involves
 417 relaxation to the X-state via a conical intersection. (3.) Following this transition, the molecule, now in a highly
 418 vibrationally excited state, may undergo isomerization to the vinylidene cation $[\text{C}=\text{CH}_2]^+$. A to and fro isomerization
 419 between acetylene and vinylidene takes places, indicated by the green double-arrow. *Dissociation pathway:* (1.b)
 420 While the 32 fs pump-pulse is present, a fifth photon can be absorbed on the A-state thus exciting population to
 421 higher lying states (presumably of a_u symmetry, see Figure S9 in the SI) which have sufficient energy to dissociate
 422 along the C=C bond. Pictograms show the molecular structure in each configuration, starting from neutral acetylene
 423 (n) in the lower left corner. After excitation, $[\text{HC}=\text{CH}]^+$ remains in linear configuration ($D_{\infty h}$), reaches the trans
 424 geometry (see Figure 5), followed by the transition state and changes to a “Y-shape” once a proton migrates from
 425 one C-atom to the other in the vinylidene structure (C_{2v}). To probe the nuclear structure, either further 266 nm
 426 photons are absorbed to reach the dication of acetylene and vinylidene (single pulse experiment) or a second time
 427 delayed 800 nm pulse leads to Coulomb explosion of the charged molecule (pump-probe experiment). With the latter
 428 we reach the doubly charged (2+), as well as the triply charged ionic states (3+) and thus correlate either two
 429 fragments (CH^+CH^+ or C^+CH_2^+) or three fragments $\text{H}^+\text{C}^+\text{CH}^+$ with each other. In the inset a sketch of the
 430 experimental setup with orientations of molecules, laser pulses and time of flight (TOF) direction towards the detector
 431 is given, with θ being the angle between molecular axis and laser polarization. Molecules being oriented parallel to
 432 the laser field correspond to $\theta=0^\circ$. Energy levels are taken from Ref. ²⁷ and our calculations.

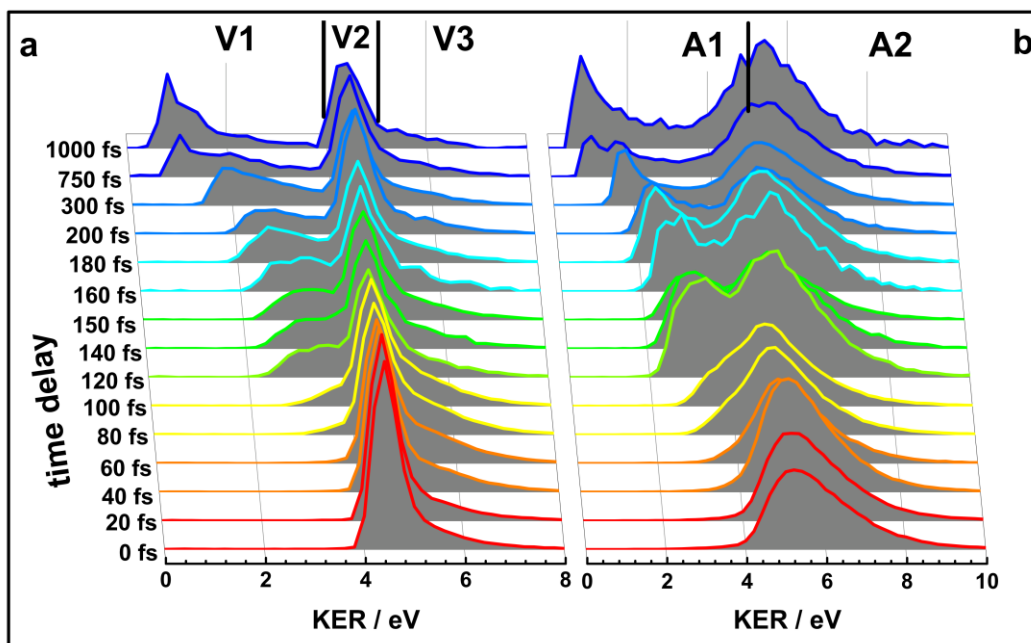


433

434 **Figure 2 – single pulse experiment:** a) Wavelength-, pulse duration- and pulse power dependence on the
 435 vinylidene yield. Filled grey curve: 800 nm excitation, 200 fs pulse duration, $1 \cdot 10^8$ W, green curve: 266 nm excitation,
 436 32 fs pulse duration, $1 \cdot 10^8$ W, red curve: 266 nm excitation, 32 fs pulse duration, $2 \cdot 10^8$ W, black curve: 266 nm
 437 excitation, 110 fs pulse duration, $0.5 \cdot 10^8$ W, blue curve: 266 nm excitation, 250 fs pulse duration, $0.4 \cdot 10^8$ W open
 438 circles: excitation with 38 eV from an FEL¹⁴. b) Cuts of the angular distribution of the 266 nm, 110 fs spectrum shown
 439 as black solid line in a). Cyan corresponds to angles between $0-25^\circ$ (note that the high energy peak exceeds the
 440 main peak here), yellow corresponds to $25-45^\circ$, orange to $45-60^\circ$ and grey to $60-90^\circ$. All curves are normalized to the
 441 peak maximum.

442

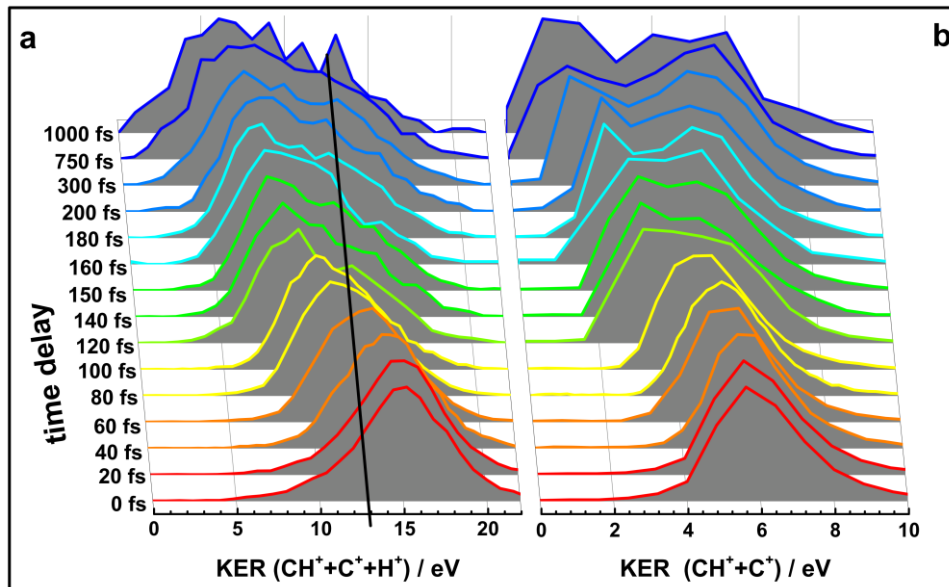
443



444
 445 **Figure 3 – Two-fragment correlation-Kinetic energy release:** Vinylidene channel $C^+ + CH_2^+$ is shown in **a** and
 446 acetylene channel $CH^+ + CH^+$ in **b** with increasing time delay from 0 fs (red) to 1000 fs (blue). The vinylidene spectrum
 447 contains three different regions: V1: the low energy range below 4 eV, V2: the intermediate energy range between 4
 448 and 5 eV and V3: the high-energy range, > 5 eV. The acetylene channel is divided into two regions, the low energy
 449 region A1: < 4 eV and the high-energy region A2: > 4 eV. Spectra are normalized by the number of correlated counts,
 450 to account for varying acquisition times at different time-steps, as well as for minor fluctuations in pulse power or gas
 451 pressure. This normalization allows comparison of the absolute count number in each channel at each time delay.

452

453



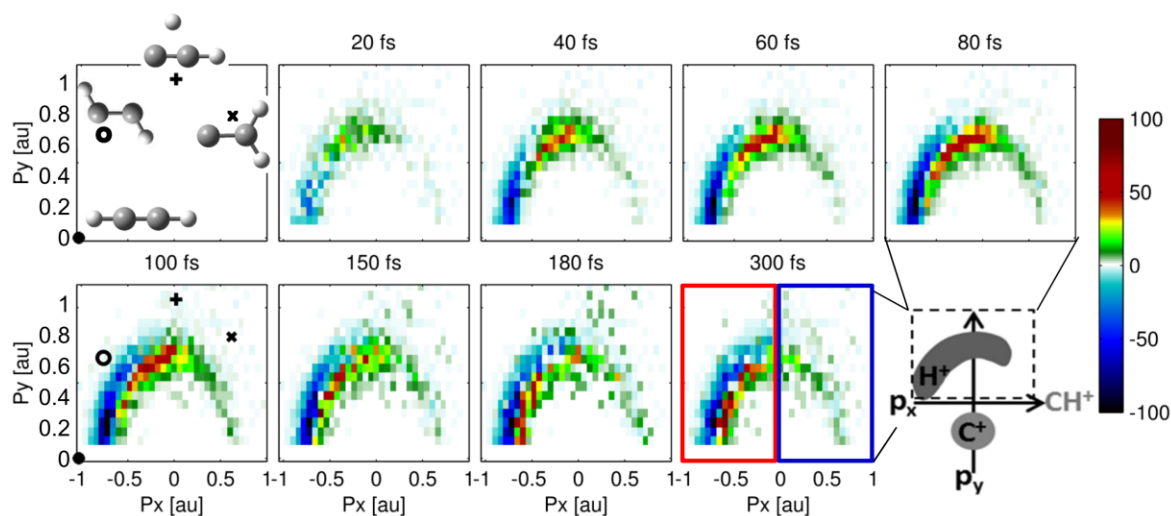
454

455 **Figure 4 – Three-fragment-correlation data-Kinetic energy release:** Peak values are normalized to the maximum.
 456 a) total KER CH⁺+C⁺+H⁺, b) KER from CH⁺+C⁺ fragments. The black line in a) indicates the energy cut-off for the
 457 Newton plots of Figure 5. Binning was adjusted according to the number of correlated counts available for each time
 458 delay.

459

460

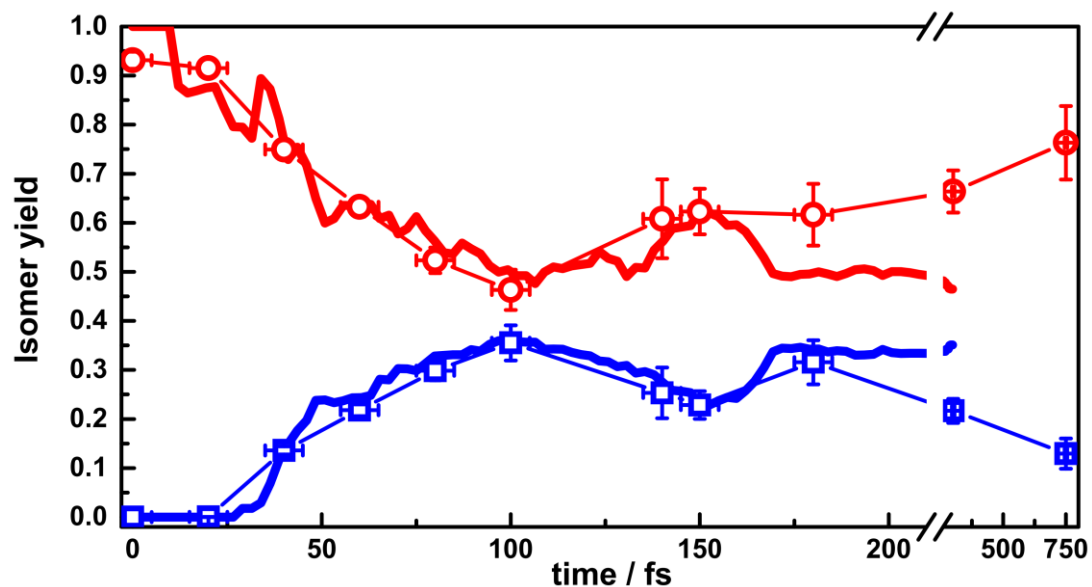
461



462

463 **Figure 5 – The molecular movie of proton migration: Newton plots filtered for KER > 13 eV.** Symbols show
 464 classically calculated results assuming Coulomb potentials for linear configuration (·), trans configuration (◦),
 465 transition state (+) and vinylidene (x), given in the upper left corner. As indicated on the lower right, all molecules are
 466 rotated such that the momentum vector of CH⁺ points towards the positive x-axis, the relative momentum of C⁺ is
 467 confined to the negative y-axis. Here, we plot only data of the momentum vector of H⁺, after subtracting the
 468 distribution at $\Delta t=0$. The plots show the evolution of H⁺ momenta with increasing time delay from 0 fs to 300 fs,
 469 normalized to the integral. The distribution appears localized at 20 fs (dark green data points) and spreads out
 470 towards the CH⁺ ion with increasing time delay. C⁺ is considerably heavier than H⁺ and thus localized, while the light
 471 H⁺ propagates with time being transferred from the acetylene configuration to the vinylidene one. White colours
 472 correspond to zero, blue colours to negative contributions (after subtraction, *i.e.* where the population originates) and
 473 other colours to positive contributions (*i.e.* where the population is going).

474



475

476 **Figure 6 – Comparison of theory (thick lines) and experiment (open symbols) for acetylene (red) and**
 477 **vinylidene (blue) yield:** Theoretical curves show the superposition of acetylene and vinylidene yield in both the
 478 ground state and excited states of the cation as a function of time (see Figure S8 in the SI for details). Experimental
 479 values are obtained by integrating the Newton plots of Figure 5 for negative P_x (acetylene, circles) or positive P_x
 480 (vinylidene, squares), as indicated there by the red and blue box at 300 fs. Note the broken axis for long time delays.
 481 Experimental data are corrected by offset and scaling factor to fit the theoretical points.

482

483

484 References:

- 485 1. Zewail, A. H. Four-dimensional electron microscopy. *Science* **328**, 187–93 (2010).
- 486 2. Weinstein, J. A. & Hunt, N. T. In search of molecular movies. **4**, 4–5 (2012).
- 487 3. Blaga, C. I. *et al.* Imaging ultrafast molecular dynamics with laser-induced electron
488 diffraction. *Nature* **483**, 194–7 (2012).
- 489 4. Haessler, S. *et al.* Attosecond imaging of molecular electronic wavepackets. *Nat. Phys.* **6**,
490 200–206 (2010).
- 491 5. Wörner, H. J., Bertrand, J. B., Kartashov, D. V, Corkum, P. B. & Villeneuve, D. M.
492 Following a chemical reaction using high-harmonic interferometry. *Nature* **466**, 604–7
493 (2010).
- 494 6. Chapman, H. N. *et al.* Femtosecond X-ray protein nanocrystallography. *Nature* **470**, 73–
495 77 (2011).
- 496 7. Miller, R. J. D. *et al.* “Making the molecular movie”: first frames. *Acta Crystallogr. A.* **66**,
497 137–56 (2010).
- 498 8. Eichberger, M. *et al.* Snapshots of cooperative atomic motions in the optical suppression
499 of charge density waves. *Nature* **468**, 799–802 (2010).
- 500 9. Barty, A., Küpper, J. & Chapman, H. N. Molecular imaging using X-ray free-electron
501 lasers. *Annu. Rev. Phys. Chem.* **64**, 415–35 (2013).
- 502 10. Légaré, F. *et al.* Imaging the time-dependent structure of a molecule as it undergoes
503 dynamics. *Phys. Rev. A* **72**, 1–4 (2005).
- 504 11. Bocharova, I. *et al.* Charge Resonance Enhanced Ionization of CO₂ Probed by Laser
505 Coulomb Explosion Imaging. *Phys. Rev. Lett.* **107**, 63201 (2011).
- 506 12. Matsuda, A., Fushitani, M., Takahashi, E. J. & Hishikawa, A. Visualizing hydrogen atoms
507 migrating in acetylene dication by time-resolved three-body and four-body Coulomb
508 explosion imaging. *Phys. Chem. Chem. Phys.* **13**, 8697–704 (2011).
- 509 13. Hishikawa, A., Matsuda, A., Fushitani, M. & Takahashi, E. J. Visualizing Recurrently
510 Migrating Hydrogen in Acetylene Dication by Intense Ultrashort Laser Pulses. *Phys. Rev.*
511 *Lett.* **99**, 258302 (2007).
- 512 14. Jiang, Y. H. *et al.* Ultrafast Extreme Ultraviolet Induced Isomerization of Acetylene
513 Cations. *Phys. Rev. Lett.* **105**, 263002 (2010).
- 514 15. Koopmans, T. Über die Zuordnung von Wellenfunktionen und Eigenwerten zu den
515 Einzelnen Elektronen Eines Atoms. *Physica* **1**, 104–113 (1934).

- 516 16. McFarland, B. K., Farrell, J. P., Bucksbaum, P. H. & Gühr, M. High harmonic generation
517 from multiple orbitals in N₂. *Science* **322**, 1232–5 (2008).
- 518 17. Akagi, H. *et al.* Laser tunnel ionization from multiple orbitals in HCl. *Science* **325**, 1364–7
519 (2009).
- 520 18. Smirnova, O. *et al.* High harmonic interferometry of multi-electron dynamics in molecules.
521 *Nature* **460**, 972–7 (2009).
- 522 19. Tilborg, J. Van *et al.* Femtosecond isomerization dynamics in the ethylene cation
523 measured in an EUV-pump NIR-probe configuration. *J. Phys. B At. Mol. Opt. Phys.* **42**,
524 081002 (2009).
- 525 20. Takahashi, E. J., Lan, P., Mücke, O. D., Nabekawa, Y. & Midorikawa, K. Attosecond
526 nonlinear optics using gigawatt-scale isolated attosecond pulses. *Nat. Commun.* **4**, 2691
527 (2013).
- 528 21. Tzallas, P., Skantzakis, E., Nikolopoulos, L. a. a., Tsakiris, G. D. & Charalambidis, D.
529 Extreme-ultraviolet pump–probe studies of one-femtosecond-scale electron dynamics.
530 *Nat. Phys.* **7**, 781–784 (2011).
- 531 22. Madjet, M. E., Li, Z. & Vendrell, O. Ultrafast hydrogen migration in acetylene cation driven
532 by non-adiabatic effects. *J. Chem. Phys.* **138**, 094311 (2013).
- 533 23. Douguet, N., Rescigno, T. N. & Orel, a. E. Time-resolved molecular-frame photoelectron
534 angular distributions: Snapshots of acetylene-vinylidene cationic isomerization. *Phys. Rev.*
535 *A* **86**, 013425 (2012).
- 536 24. Jiang, Y. H. *et al.* Ultrafast dynamics in acetylene clocked in a femtosecond XUV
537 stopwatch. *J. Phys. B At. Mol. Opt. Phys.* **46**, 164027 (2013).
- 538 25. Wells, E. *et al.* Adaptive strong-field control of chemical dynamics guided by three-
539 dimensional momentum imaging. *Nat. Commun.* **4**, 2895 (2013).
- 540 26. Alnaser, A. *et al.* Momentum-imaging investigations of the dissociation of D₂⁺ and the
541 isomerization of acetylene to vinylidene by intense short laser pulses. *J. Phys. B At. Mol.*
542 *Opt. Phys.* **39**, S485–S492 (2006).
- 543 27. Boyé-Péronne, S., Gauyacq, D. & Liévin, J. Vinylidene-acetylene cation isomerization
544 investigated by large scale ab initio calculations. *J. Chem. Phys.* **124**, 214305 (2006).
- 545 28. Lezius, M. *et al.* Nonadiabatic Multielectron Dynamics in Strong Field Molecular Ionization.
546 *Phys. Rev. Lett.* **86**, 51–54 (2001).
- 547 29. Madjet, M. E.-A., Vendrell, O. & Santra, R. Ultrafast Dynamics of Photoionized Acetylene.
548 *Phys. Rev. Lett.* **107**, 263002 (2011).

- 549 30. Zyubina, T. S., Dyakov, Y. a, Lin, S. H., Bandrauk, a D. & Mebel, a M. Theoretical study
550 of isomerization and dissociation of acetylene dication in the ground and excited
551 electronic states. *J. Chem. Phys.* **123**, 134320 (2005).
- 552 31. Xu, H. *et al.* Two-proton migration in 1,3-butadiene in intense laser fields. *Phys. Chem.*
553 *Chem. Phys.* **12**, 12939–42 (2010).
- 554 32. Wales, B. *et al.* Multiple ionization and complete fragmentation of OCS by impact with
555 highly charged ions Ar 4+ and Ar 8+ at 15 keV q -1. *J. Phys. B At. Mol. Opt. Phys.* **45**,
556 045205 (2012).
- 557 33. Schmidt, B. E. *et al.* Poor man's source for sub 7 fs: a simple route to ultrashort laser
558 pulses and their full characterization. *Opt. Express* **16**, 18910–18921 (2008).
- 559 34. Wales, B. *et al.* A coincidence detection algorithm for improving detection rates in
560 Coulomb Explosion Imaging. *Nucl. Instruments Methods Phys. Res. Sect. A Accel.*
561 *Spectrometers Detect. Assoc. Equip.* **667**, (2011).
- 562 35. Ben-Nun, M. & Martínez, T. J. Ab Initio Quantum Molecular Dynamics. *Adv. Chem. Phys.*
563 **121**, 439–512 (2002).
- 564 36. Lischka, H. *et al.* COLUMBUS, an ab initio electronic structure program, release 7.0.
565 (2012). at <<http://www.univie.ac.at/columbus/>>
- 566 37. J.F. Stanton, J. Gauss, M.E. Harding, P. G. S. *et al.* CFOUR, a quantum chemical
567 program package written by: at <For the current version, see <http://www.cfour.de>.>

568